Reduction of Te-rich phases in $Cd_{1-x}Zn_xTe$ ($x = 0.04$) crystals

2002 J. Phys.: Condens. Matter 14 10183

(http://iopscience.iop.org/0953-8984/14/43/315)

INSTITUTE OF PHYSICS PUBLISHING JOURNAL OF PHYSICS: CONDENSED MATTER

J. Phys.: Condens. Matter **14** (2002) 10183–10191 PII: S0953-8984(02)39484-0

Reduction of Te-rich phases in $Cd_{1-x}Zn_xTe$ ($x = 0.04$) crystals

Li Yujie[1,2] **and Jie Wanqi**[1]

[1] The State Key Laboratory of Solidification Processing, Northwestern Polytechnical University, Xi'an 710072, People's Republic of China
[2] Physics Department, Peking University, Beijing 100871, People's Republic of China

Received 15 July 2002
Published 18 October 2002
Online at stacks.iop.org/JPhysCM/14/10183

Abstract

$Cd_{1-x}Zn_xTe$ crystals are annealed in Cd/Zn vapours to eliminate Te-rich phases. During the saturated Zn partial pressure annealing and the high-temperature annealing under low P_{Zn}, large Te-rich phases gather at the slice surface through thermo-migration. This process increased the stress in the bulk crystals and caused the formation of defects such as twins, stacking faults, and dislocations. The IR transmission is greatly improved by annealing the slices under saturated P_{Zn} and then removing a layer from the surface of the slices with a thickness of about 50 μm. For $Cd_{1-x}Zn_xTe$ slices annealed at low temperature and low Zn partial pressure, the reduction of the Te-rich phases greatly depends on the diffusion of the atomic defects.

1. Introduction

The II–VI semiconductor $Cd_{1-x}Zn_xTe$ has a wide variety of applications including in x-ray or γ-ray detectors and the epitaxial growth of HgCdTe infrared (IR) detector wafers, especially $Cd_{1-x}Zn_xTe$ with $x = 0.04$. Bulk crystals of $Cd_{1-x}Zn_xTe$ with high quality are very difficult to obtain. Commercial $Cd_{1-x}Zn_xTe$ crystals usually contain defects such as twins, sub-grain boundaries, dislocations, and Te-rich phases. These defects, especially Te-rich phases, will seriously degrade the optical and electrical properties of the crystals. Two kinds of Te-rich phase exist in $Cd_{1-x}Zn_xTe$ crystals, namely Te precipitates and Te inclusions. They form through different mechanisms. At high temperature, a relatively large amount of excess Te dissolves in $Cd_{1-x}Zn_xTe$ and exists as point defects. The solubility of Te decreases as the temperature decreases. The excess Te forms Te precipitates. For growth from a $Cd_{1-x}Zn_xTe$ melt, the solid–liquid interface tends to be unstable. The Te-rich droplets will be trapped by the growing interface. After solidification, Te inclusions appear at the position of the Te-rich droplets included.

Te precipitates and Te inclusions are distinguished by their size. Usually, Te precipitates are in the range 10–30 nm [1]. Direct observation and measurement of the precipitates are very difficult. They cannot be 'seen' by the metallography method. The IR spectra of $Cd_{1-x}Zn_xTe$

Table 1. The parameters for annealing experiments.

Slice no	Heating rate (°C h^{-1})	T_1[a] (°C)	T_2[b] (°C)	Time (h)	Concentration of the reservoir (mg)	Notes
1	70	700	650	40	Cd(198) + Zn(3.1)	Saturated-P_{Zn}
2	50	500	400	60	Cd(444) + Zn(11.1)	annealing
3	140	700	500	40	$Cd_{0.995}Zn_{0.005}$	High-temperature
4	140	700	500	100	$Cd_{0.995}Zn_{0.005}$	annealing in low P_{Zn}
5	70	700	500	40	$Cd_{0.995}Zn_{0.005}$	
6	50	500	400	40	$Cd_{0.999}Zn_{0.001}$	Low-temperature
7	50	500	400	100	$Cd_{0.995}Zn_{0.005}$	annealing in low P_{Zn}

[a] T_1: slice temperature.
[b] T_2: Cd reservoir temperature.

slices indirectly show the density and the distribution of Te precipitates [2]. Te inclusions are much larger. Their dimensions are usually larger than 1 μm [3–6]. Larger inclusions can be several hundred micrometres and can be easily shown by etching with appropriate etchants.

Te-rich phases existing in the as-grown $Cd_{1-x}Zn_xTe$ crystals are reduced by annealing the slices in Cd or CdZn vapour. The aim of this paper is to find the appropriate annealing conditions for eliminating Te-rich phases and improving the properties of the crystals.

2. Experimental procedure

$Cd_{1-x}Zn_xTe$ crystals with $x = 0.04$ and diameter 30 mm were grown by the vertical Bridgman method modified with the accelerated crucible rotation technique (ACRT-B) in our laboratory. The temperature gradient at the growing interface was 10 °C cm^{-1}. The crystals were cut into 1 mm thick slices and mechanically polished on both sides.

As-grown slices with dense and large Te-rich phases were chosen in the experiments for the purpose of revealing the variation of Te inclusions in morphology and size. After etching with E and E_{Ag} solutions [7], Te inclusions are clearly seen using SEM (scanning electronic microscopy). The IR spectra of the slices before and after annealing were measured to show the influence of the heat treatment on Te precipitates. Three classes of annealing conditions, including annealing in saturated Zn partial pressure, high-temperature annealing in low Zn partial pressure, and low-temperature annealing in low Zn partial pressure, were applied according to our theoretical analysis in our former papers [8, 9]. The detailed annealing parameters are shown in table 1. The reservoir metals Cd + Zn or $Cd_{1-y}Zn_y$ are designed to maintain the required Cd and Zn partial pressure.

For each of the six experiments, the Cd partial pressure (P_{Cd}) was kept within the existence region of $Cd_{0.96}Zn_{0.04}Te$ according to the P–T phase diagram [10]. The Zn partial pressure (P_{Zn}) for the saturated Zn partial pressure annealing is one order higher than the upper limit of P_{Zn} in the P–T phase diagram. High-temperature annealing in low Zn partial pressure was designed to keep the slices at 700 °C and P_{Zn} within the existence region of $Cd_{0.96}Zn_{0.04}Te$. The upper and lower limits of the partial pressure for Te, Zn, and Cd elements defined by the three-phase loops of $Cd_{0.96}Zn_{0.04}Te$ are varied with the temperature of the slices in the P–T phase diagrams. Thus, for low-temperature annealing in low Zn partial pressure, although the temperature for the slice and the reservoir are noted to be 500 and 400 °C respectively, the condition of P_{Zn} for this group of annealing parameters is the same for as high-temperature annealing in low Zn partial pressure.

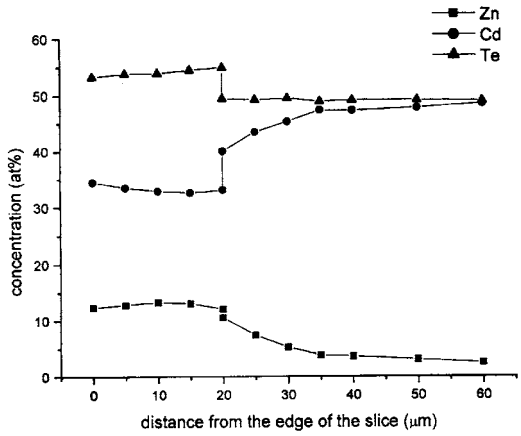

Figure 1. The concentration profiles measured on the cross-section of slice No 1.

3. Results and discussion

3.1. Saturated-P_{Zn} annealing

3.1.1. Concentration distribution in the surface layer. Both No 1 and No 2 slices were annealed in saturated Zn partial pressure despite the difference in annealing temperature. After annealing, surface layers with thicknesses of 17–27 μm were formed on both of these samples according to the concentration profiles measured on the cross-section of the annealed slices for Zn, Cd, and Te as shown in figure 1 [8]. A sharp change takes place at the boundary located between the surface layers and the bulk crystals. In the surface layer, the concentration of Zn is higher than 10 at.%. It corresponds to $x \geqslant 0.2$, while the original concentration of the bulk crystal is $x = 0.04$. In addition, the concentration of Te in the surface layer, which amounts to 54–69 at.%, is also much higher than that in the bulk crystal.

3.1.2. Thermo-migration of Te-rich phases and its effects on other defects. Systematic etching experiments were carried out to show the microstructures in slices No 1 and No 2. Table 2 describes various microstructures observed in them at different positions along the direction perpendicular to the slice surface. SEM photos of these typical microstructures are shown in figure 2. Careful study led to the conclusion that the regular distribution was closely related to the migration of the Te-rich phases.

During the heating period of the annealing process, the temperature on the slice surface is higher than that of the centre part of the slice. The temperature gradient points to the surface. As long as the temperature is higher than the melting point of Te at some part of the slice, Te-rich phases located there are melted into Te-rich droplets. These droplets migrate along the temperature gradient and gather at positions adjacent to the slice surface. This process could occur as a result of the dissolution of $Cd_{0.96}Zn_{0.04}Te$ in Te droplets at the higher-temperature ends and precipitation at the lower-temperature ends. The diffusion coefficient of Cd and Zn in liquid Te is high enough to support this mechanism [11]. The slices in this experiment are cut on the (111) plane and the thermo-migration direction of the droplets is perpendicular to the (111) plane. The precipitation of $Cd_{0.96}Zn_{0.04}Te$ at the lower-temperature end of the Te-rich droplets resembles the homogeneous epitaxial growth of $Cd_{0.96}Zn_{0.04}Te$ on (111) $Cd_{0.96}Zn_{0.04}Te$ substrates.

Table 2. The distribution of different microstructures in the depth direction of the slices annealed under saturated Zn partial pressure. The observation plane is (111); 'con.' stands for concentration.

Distance from the surface (μm)	Te-rich strips	Dislocation associations	EPD of the scattering dislocations (cm^{-2})	Layered structures	Te-rich phases
0–25		—	(The surface layer)		
25–30 (figure 2(a))	The crossing angles are 60° or 120°; Te con.: >70 at.%	—	—	—	—
28–35 (figure 2(b))	— —	With small-angle grain boundaries, in which Te con. is >80 at.%	4.7×10^5–10^6 (in the etch pits, Te con. is >80 at.%)	—	—
35–42 (figure 2(c))	—	A few small-angle grain boundaries, which are not rich in Te	$>1 \times 10^7$ (the etch pits are not rich in Te)	Large amount of layered structures, with the crossing angles of 60°	—
42–50 (figures 2(d), (e))	— —	— —	— —	Layered strips	In the layered structures
>50 (figure 2(f))	—	—	—	A few —	Next to the layered structures

If the stacking order of the (111) plane meets faults, a stacking fault will occur. The nuclei of the stacking faults grow in the shape of an upside-down tetrahedron. After etching, the stacking faults appear as triangular-layered structures with crossing angles of 60°, as shown in figures 2(c)–(f). The quantity of the layered structures that appear at a certain location is determined by the size of the Te-rich droplets removed. Figure 3 is a diagrammatic sketch of the growth of the stacking faults and their morphology observed on the (111) plane.

Te-rich droplets migrate as thin discs (figure 4). Their dimension normal to the migration direction (denoted by L) increases as the droplets get closer to the slice surface. When they arrive at the position where the distance from the original slice surface is 28–35 μm, L becomes very large. The stress in the crystal at the same location increases rapidly and causes the multiplication of dislocations. In regions with high densities of dislocations, small-angle grain boundaries tend to be formed (figure 2(b)). The Te-rich droplets continue to move. At the position at a distance of 25–30 μm from the surface, L becomes larger and correspondingly the stress at this site mounts still higher, and twins are formed. In $Cd_{0.96}Zn_{0.04}Te$ the first twins were {111}–{111} and {112}–{112} twins. The morphology of two crossed twins is shown on the {111} plane as strips with the crossing angles of 60° or 120° (as shown in figure 2(a)).

Te-rich phases tend to accumulate near twins, dislocations, and small-angle grain boundaries. Thus the concentrations measured near those defects are rich in Te. Te-rich phases migrate to and gather near the slice surface and are gradually reduced by reacting with the interdiffusing Cd and Zn from the vapour phase. The Te-rich phases with large dimensions, i.e. Te inclusions, in the bulk crystal are eliminated as a result of this process.

The Te precipitates are too small to migrate because of the high interface energy. However, the greater the driving force of the thermo-migration, the smaller the smallest Te-rich droplets

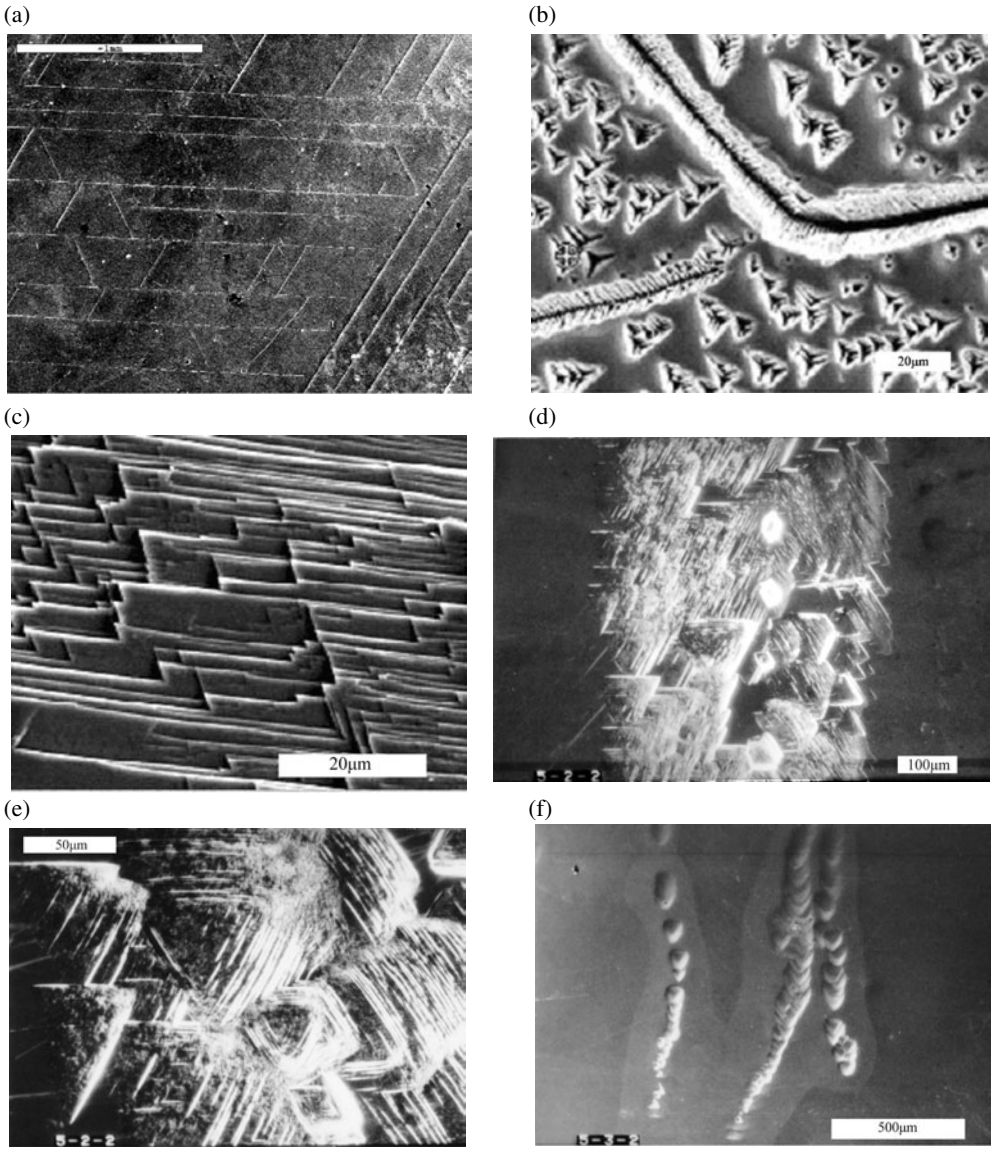

Figure 2. (a) Te-rich strips locate at a depth of 25–30 μm. (b) The small-angle grain boundaries and the dislocations observed at a depth of 28–35 μm; $\oplus$ shows the measurement position for the concentration. (c) Typical layered structure in the bulk crystal at a depth of 35–42 μm. (d) Layered structure locates in the bulk crystal at a depth of 42–50 μm. (e) An enlargement of the strip shown in (d). (f) A small amount of layered structure lying at the centre of the slices locates at a depth greater than 50 μm.

that can migrate. Also, the migrating Te droplets can entrap Te precipitates on their way to the surface and reduce the density of the Te precipitates. The larger the quantity of Te-rich phases participating in the migration, the better this mechanism works in reducing Te precipitates. We compared the IR spectra of slice No 1 before and after the annealing in saturated Zn partial pressure in figure 5. Before the IR spectra of the annealed slice were measured, the slice was

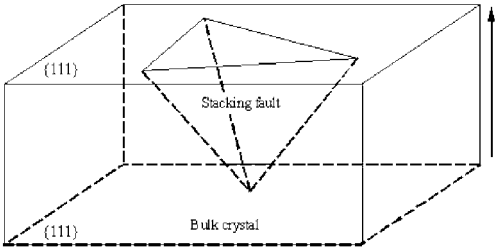

Figure 3. The stacking fault nucleates and grows at the lower-temperature end of the migrating Te-rich droplet and its morphology observed on {111} plane; ↑ denotes the thermo-migration direction of the Te-rich phases, which is the same as the direction of the temperature gradient.

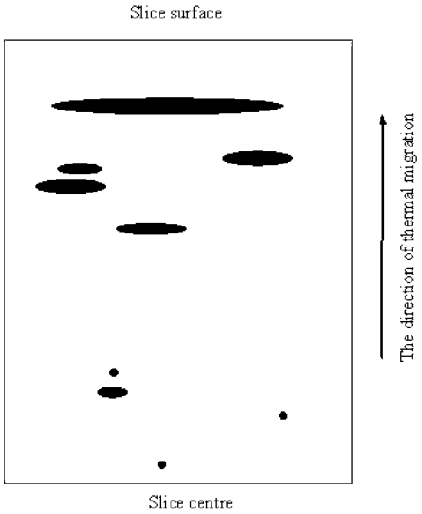

Figure 4. Te-rich droplets that migrated as thin discs.

mechanically polished to remove a layer of 50 μm to eliminate the influence of the surface layer and the Te-rich-phase accumulated layer of the bulk crystal. The most noticeable phenomenon is that the IR transmittance of the bulk crystal rises considerably upon annealing, in spite of the influence of the change in slice thickness.

All in all, after annealing in saturated P_{Zn} and removing a layer of 50 μm from the slice surface, the Te-rich phases, including both Te precipitates and the Te inclusions, in the bulk crystals are mostly removed and the IR transmission is obviously improved.

3.2. High-temperature annealing in low P_{Zn}

For slices Nos 3–5 annealed at high temperature and low P_{Zn}, no such surface layer formed on the slice surfaces. After etching, large Te inclusions were found on the surface (figure 6). The area percentage of the Te-rich phases over the whole observation area is about 15%. On increasing the heating rate of the annealing process from 70 to 140 °C h^{-1}, bulk Te inclusions in figure 6 were replaced by net-shaped Te-rich phases existing adjacent to the small-angle grain boundaries, which occupy about 20% of the observed area on the slice surface (figure 7).

In slices annealed at high temperature and low P_{Zn}, Te inclusions migrate in the same way as those in the slices annealed in saturated P_{Zn}. The increased heating rate causes stronger

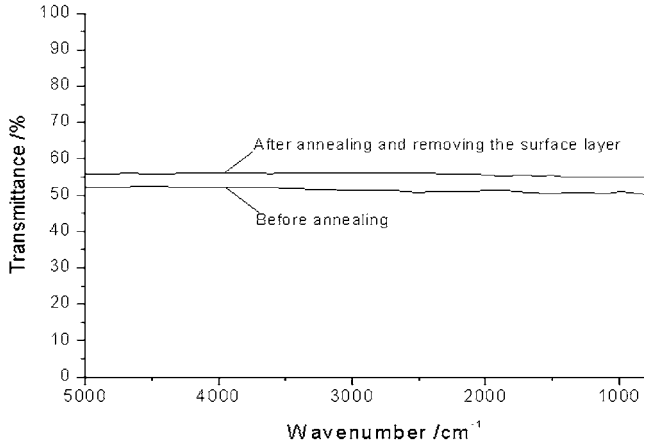

Figure 5. The IR transmission spectra of slice No 1 before and after annealing.

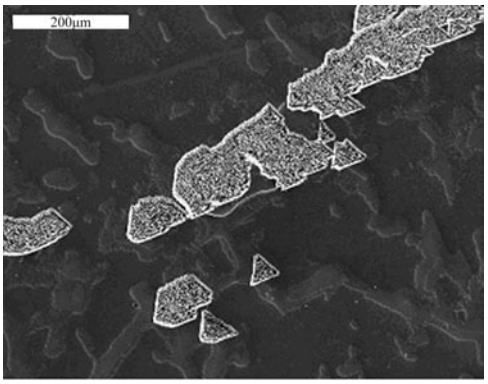

Figure 6. The large Te-rich phase on the surface of slice No 5 after annealing (the heating rate is 70 °C h^{-1}, and the annealing time is 40 h).

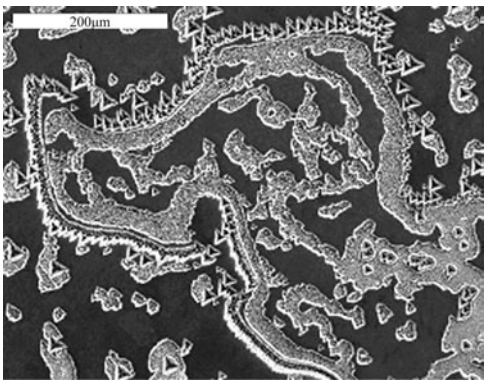

Figure 7. The small-angle grain boundaries and the nearby net-shaped Te-rich phases (the heating rate is 140 °C h^{-1}, and the annealing time is 40 h).

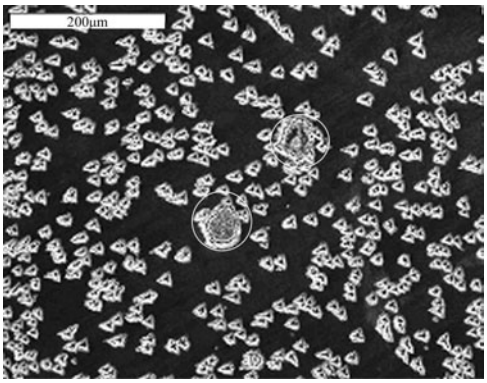

Figure 8. The scattering dislocation etch pits and small Te-rich phases (outlined with a circle) in slice No 4 after annealing (the heating rate is 140 °C h^{-1}, and the annealing time is 100 h).

thermo-migration and results in greater amounts of Te inclusions gathered on the surface. A prolonged annealing process permits the Te inclusions moved to the slice surface to equilibrate for longer with the outside vapour pressure and this results in the gradual elimination of the inclusions. Thus, after annealing for 100 h, only a few inclusions with dimensions smaller than 50 μm are left on the slice surface (figure 8). The etch pit density in figure 8 is (4–8) $\times$ 10^5 cm^{-2}. The IR transmission was not improved much upon annealing. The strength of the thermo-migration under this annealing condition is much weaker than that under the annealing condition with saturated P_{Zn}. Considerable quantities of Te-rich phases, especially Te precipitates, remained in the bulk crystals.

3.3. Low-temperature annealing in low P_{Zn}

After annealing at low temperature and low P_{Zn}, no inclusions were found to accumulate near the surface in slices Nos 6 and 7. This indicates that the thermo-migration of the Te-rich phases was very weak. The elimination of the Te-rich phases was greatly dependent on the process of diffusion of the atomic defects, such as interdiffusion of Cd and Zn interstitials and out-diffusion of Cd vacancies.

Annealing for a very long time was needed to improve the IR transmittance. However, in figure 9, the etch pit density in the bulk crystals was found to decrease from 4 $\times$ 10^5 cm^{-3} before annealing to about 1 $\times$ 10^4 cm^{-2} after annealing.

4. Conclusions

(1) Large Te-rich phases gather at the slice surface through thermo-migration during the saturated Zn partial pressure annealing, and the high-temperature annealing in low P_{Zn}. The migration process increased the stress in the bulk crystals and caused the formation of twins, stacking faults, and dislocations with high densities. The stronger the thermo-migration, the better the results as regards eliminating Te-rich phases, including both Te inclusions and Te precipitates.

(2) The thermo-migration process was very weak in slices annealed at low temperature and low Zn partial pressure. Under this annealing condition, the elimination of the Te-rich phases greatly depends on the diffusion of the atomic defects.

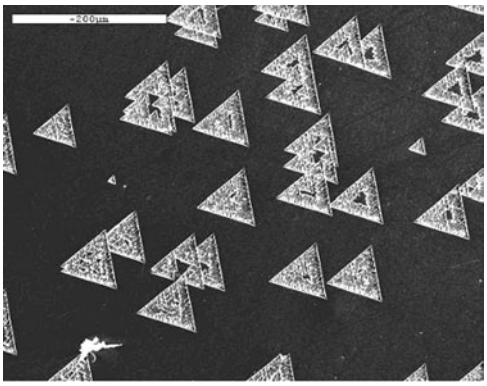

Figure 9. The distribution of the dislocation etch pits in slice No 7 annealed at low temperature and low Zn partial pressure for 100 h.

(3) In order to eliminate Te-rich phases and to improve IR permeability, the most efficient process should be annealing the slices in saturated P_{Zn} and then removing a layer from the surface of the slices with a thickness of about 50 μm.

References

[1] Rudolph P, Neubert M and Mühlberg M 1993 *J. Cryst. Growth* **128** 582
[2] Yadava R D S, Sundersheshu B S, Anandan M, Bagai R K and Borle W N 1994 *J. Electron. Mater.* **23** 1349
[3] Azoulay M, Petter S and Gafni G 1990 *J. Cryst. Growth* **101** 256
[4] Shen J, Aidum D K, Regel L and Wilcox W R 1993 *J. Cryst. Growth* **132** 250
[5] Johnson C J 1989 *Proc. SPIE* **1106** 56
[6] Mullin J B and Stranghan B W 1997 *Revue Phys. Appl.* **12** 267
[7] Inoue M, Teramoto I and Takayanagi S 1963 *J. Appl. Phys.* **34** 404
[8] Li Yujie, Zhang Xiaona and Jie Wanqi 2001 *Acta Phys. Sin.* **50** 2327
[9] Li Yujie 2002 *DEng Thesis* Northwestern Polytechnical University
[10] Yu T C and Brebrick R F 1993 Phase diagrams of CdTe/CdZnTe *Properties of Narrow Gap Cadmium-Based Compounds (Inspec Datareviews Series, No 10)* ed P Capper (London: Inspec) p 413
[11] Schwarz R and Benz K W 1994 *J. Cryst. Growth* **144** 150